Article

Nano-Sized Polyelectrolyte Complexes Formed between Poly(vinyl benzyl trimethyl ammonium chloride) and Insulin

Angeliki Chroni [ID] and Stergios Pispas *[ID]

Theoretical and Physical Chemistry Institute, National Hellenic Research Foundation,
48 Vassileos Constantinou Avenue, 11635 Athens, Greece; angelikechrone@gmail.com
* Correspondence: pispas@eie.gr; Tel.: +30-210-727-3824

Abstract: Novel biohybrid homo-polyelectrolyte-based nanocarriers were formed by the complexation of insulin (INS) with a biocompatible and cationic polyelectrolyte, namely, poly(vinyl benzyl trimethylammonium chloride) (PVBTMAC). According to light-scattering techniques, the hydrophilic PVBTMAC homo-polyelectrolyte forms single chains in aqueous media. The resulting biohybrid PVBTMAC/INS nanocarriers were formed via electrostatic co-assembly. The effects of polyelectrolyte structure and content on the characteristics of the formed PVBTMAC/INS complexes were studied. A significant aggregation tendency of the PVBTMAC/INS complexes was observed, based on the physicochemical results, especially at high protein concentration, corroborating the effective electrostatic interaction of INS with the cationic polyelectrolyte. The physicochemical properties of the formed PVBTMAC/INS nanocarriers depended on the concentration of the stock polymer and INS solutions. A neat PVBTMAC homo-polymer and PVBTMAC/INS nanocarriers demonstrated good serum stability in the presence of fetal bovine serum (FBS) proteins. Fluorescence spectroscopy (FS) studies revealed no INS conformational changes after its complexation with the cationic PVBTMAC polyelectrolyte. The obtained PVBTMAC/INS complexes demonstrated considerable and promising characteristics for potential use as insulin delivery systems.

Keywords: cationic polyelectrolyte; polyelectrolyte–protein complexes; polyelectrolyte–insulin complexes; insulin; nanocarrier

1. Introduction

Protein-containing polyelectrolyte complexes (PECs) stand out as promising biorelevant nanoparticulate structures due to their applications in drug delivery, food science, protein purification, and enzymatic nanoreactors [1–6].

Polyelectrolytes (PEs) are usually water-soluble polymers with a net negative (polyanions) or positive (polycations) charge, depending on the pH [7]. Furthermore, PEs play a crucial role in determining the phase boundary and the possibility of liquid–liquid (complex coacervation) or solid–liquid (precipitation) phase separation [8].

Proteins, on the other hand, are polyampholytes which commonly adopt a globular folded structure, having a low charge density. They may undergo macrophase separation by either direct phase separation with an oppositely charged polymer, or by microphase segregation in the coacervate phase formed by two Pes [9].

According to PE complexation, the oppositely charged PEs associate and release bound counterions so as to decrease the free energy of the solution. Protein/PE mixtures in aqueous solutions interact electrostatically and assemble together to form PECs, whose properties depend strongly on the molecular weights of the components, densities of ionic groups, mixing ratio, concentrations, pH value and ionic strength [10]. The major driving force of protein–PE complexation are electrostatic interactions between the PE chains and the oppositely charged compounds, such as insulin (INS) [11].

In the last two decades, there has been increasing interest in the application of homo-polymers for the formation of PECS, using conventional self-assembly approaches, given their relative ease of synthesis compared to diblock co-polymer analogues. Currently, there is a handful of studies dealing with the interaction of chitosan, the most common polycation used in the formulation of PECS, with INS for oral administration. Chitosan and its derivatives are very useful in the oral delivery of hydrophilic macromolecules, due to their ability to facilitate protein transport across gut epithelial cells in vitro through paracellular/transcellular routes [12,13]. However, chitosan is soluble only in acidic pH conditions, at which it is also cationic and in an uncoiled state, judging from its low pKa value (5.5), rendering the release of protein drugs very challenging.

Therefore, Gao at al. utilized poly(glycerol methacrylate)s (PGOHMAs) cationic polymers as alternatives to chitosan for the formation of PECs [14]. In addition, Cheng et al. introduced the development of novel comb-shaped amphiphilic polymers based on polyallylamine (PAA) in the oral delivery of INS [15].

Hitherto, common PECs are highly unstable in the gastric fluid, since electrostatic interactions may be lost by fluctuations in the charge of the INS moiety at acidic pHs [16]. A process to mitigate their instability in gastric fluid could be the utilization of aromatic homo-PEs with relatively hydrophobic pendant groups, such as phenyl or benzyl moieties, so as to confer an optimum balance between hydrophilic and lipophilic properties to the formation of PECs.

The main focus of the work presented here is to create novel protein-delivery systems utilizing a biocompatible and cationic homo-PE, namely, the poly(vinyl benzyl trimethylammonium chloride) (PVBTMAC), synthesized by reversible-addition fragmentation chain transfer (RAFT) polymerization, for the electrostatic complexation with INS. The PVBTMAC homo-polymer is considered highly suitable for a wide range of biomedical applications [17], having a strong positive charge at every repeating unit and a relatively hydrophobic benzyl side group. Protein-based polymeric nanocarriers were formed by electrostatic interactions between negatively charged INS molecules and PVBTMAC. Physicochemical analysis of the RAFT synthesized PVBTMAC homo-polymer and the prepared homo-polymer/INS complexes was evaluated by static, dynamic and electrophoretic light-scattering techniques (SLS, DLS, ELS). DLS-stability studies estimated the colloidal stability of neat homo-polymer and homo-polymer/INS complexes in fetal bovine serum (FBS) to gain an accurate and deep understanding of FBS protein-homo-polymer and FBS protein-homo-polymer/INS complexes interactions in a biological milieu. In addition, attenuated total reflection-Fourier transform infrared (ATR-FTIR) and fluorescence (FS) spectroscopies were utilized to further confirm the efficient complexation of INS with the homo-PE and to address any INS conformational changes after its complexation with PVBTMAC.

2. Materials and Methods

2.1. Materials

The synthesis of PVBTMAC was performed using vinyl benzyl trimethylammonium chloride (VBTMAC, 98%, Sigma-Alrdrich, Athens, Greece) as the monomer, 4,4-Azobis(4-cyanovaleric acid) (ACVA, Sigma-Aldrich, Athens, Greece) as the radical initiator and 4-cyano-4-(phenylcarbonothioylthio) pentanoic acid (CPAD, Sigma-Aldrich, Athens, Greece) as the chain transfer agent, respectively. Recombinant human insulin (INS, Sigma-Aldrich, Athens, Greece) of molecular weight 5800 $g \cdot moL^{-1}$ was used as received. Dimethyl sulfoxide (DMSO, ≥99.9%, Sigma-Aldrich, Athens, Greece), sodium chloride (NaCl, ≥99.0%, Sigma-Aldrich, Athens, Greece), phosphate-buffered saline tablets (PBS, 98%, Sigma-Aldrich, Athens, Greece), fetal bovine serum (FBS, Sigma-Aldrich, Athens, Greece) and water for injection (WFI, 99%, Sigma-Aldrich, Athens, Greece) were also used as received.

2.2. Synthesis and Preparation of PVBTMAC Homo-Polymer

The synthesis of PVBTMAC homo-polymer was performed by RAFT and it has been described in detail in a previous work [18]. The PVBTMAC polyelectrolyte was directly

diluted with 0.01 M NaCl (using WFI) at 5×10^{-4} g·mL^{-1}. The homo-polymer stock solution was filtered using hydrophilic PVDF filters of 0.45 µm pore size.

2.3. Preparation of PVBTMAC/INS Complexes

A graphical illustration of the preparation protocol of the PVBTMAC/INS complexes is presented in Scheme 1. Indicatively, the PVBTMAC/INS biohybrid complexes were formed by dropwise addition of INS solution (1.8×10^{-2} g·mL^{-1} in DMSO) to the PVBTMAC aqueous solution (5×10^{-4} g·mL^{-1} at 0.01 M NaCl solution) under gentle stirring for 20 min at room temperature. In particular, four $(-)$INS/$(+)$pol charge ratios in the 0.25–1 range of the PVBTMAC/INS complexes were prepared (according to calculations based on the charge ratios between INS and PVBTMAC) by maintaining the volume of the polymeric solution stable in every ratio at ambient temperature under stirring. The mixed solutions were diluted with 0.01 M NaCl to obtain a final volume of 10 mL. The exact volume of PVBTMAC, INS and 0.01 M NaCl that were mixed for the preparation of 0.25, 0.5, 0.75 and 1 $(-)$INS/$(+)$pol charge ratios are reported in Table 1.
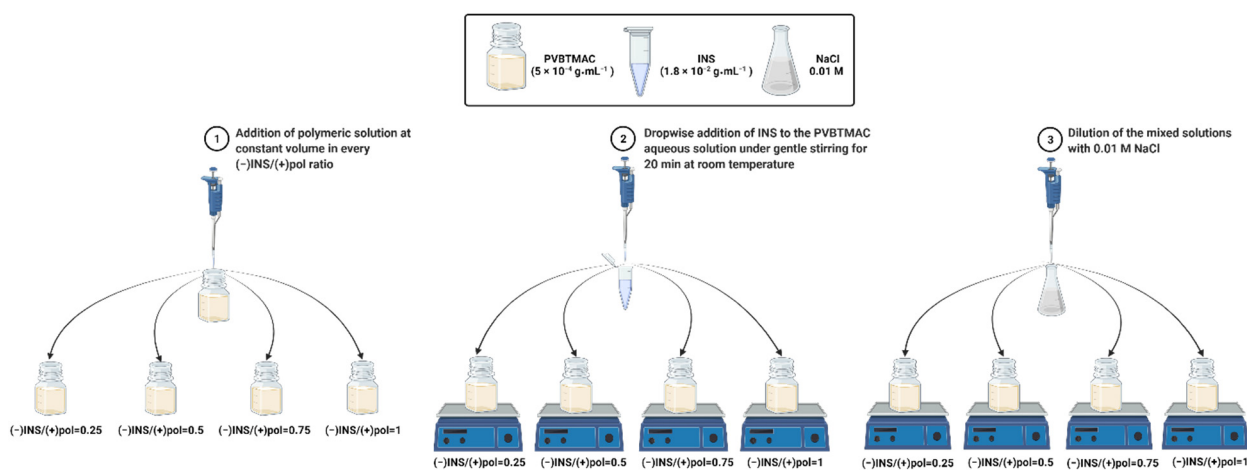
Scheme 1. Graphical illustration of the preparation of biohybrid PVBTMAC/INS complexes at 0.25, 0.5, 0.75 and 1 $(-)$INS/$(+)$pol charge ratios.

Table 1. Volumes of PVBTMAC, INS and 0.01 M NaCl required for the preparation of 0.25, 0.5, 0.75 and 1 $(-)$INS/$(+)$pol charge ratios.

$(-)$INS/$(+)$pol	$V_{PVBTMAC \text{ (mL)}}$	$V_{INS \text{ (mL)}}$	$V_{NaCl \text{ (mL)}}$	$V_{final \text{ (mL)}}$
0.25	2	0.380	7.6	10
0.5	2	0.285	7.7	10
0.75	2	0.19	7.8	10
1	2	0.095	7.9	10

2.4. FBS Interaction with PVBTMAC Homo-Polymer and PVBTMAC/INS Complexes

The mixed solutions of PVBTMAC homo-polymer and PVBTMAC/INS complexes with clarified FBS were prepared at FBS:PBS (1/9 *v/v*) ratio (PBS: phosphate buffer saline solution, pH = 7.4, ionic strength 0.154 M). The PVBTMAC homo-polymer and the PVBTMAC/INS complexes were diluted with PBS at 5×10^{-4} g·mL^{-1}. Specifically, 50 µL of each polymer sample were mixed with 3 mL of the FBS:PBS (1/9 *v/v* ratio) solution [19]. The mixtures of FBS-PVBTMAC and FBS-PVBTMAC/INS were filtered using hydrophilic PVDF filters of 0.45 µm pore size, before measurements.

2.5. Methods

The principles, instrumentations and system-equipment components of the DLS, SLS, ELS, FS and ATR-FTIR physicochemical techniques used here, are described in detail in our previous work [20].

Ionic strength effects on neat PVBTMAC homo-polymer and PVBTMAC/INS complexes were studied using the DLS method. Each sample was diluted with suitable quantities of NaCl 1 M stock solution, thus increasing salt concentration (in the range 0.01–0.5 M NaCl) in the aqueous homo-polymer and homo-polymer/INS solutions.

3. Results and Discussion

3.1. Synthesis of PVBTMAC Homo-Polymer

The synthetic process and the molecular characteristics of the PVBTMAC homo-polymer, using RAFT polymerization, are reported in previous works [17,18]. The chemical structure of the homo-polymer is shown in Scheme 2 (molecular weight from stoichiometry 39,600 g/mol).
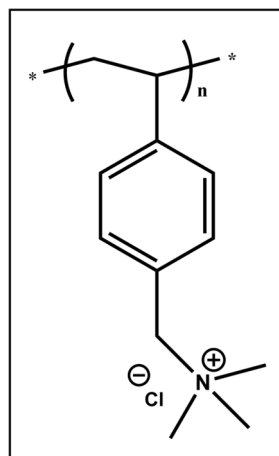

Scheme 2. Chemical structure of PVBTMAC homo-polymer synthesized by RAFT polymerization. The "*" refers to the repeating units of the polymer.

3.2. Physicochemical Characterization of PVBTMAC Homo-Polymer and PVBTMAC/INS Complexes

The size, mass, surface charge and chemical structure of PVBTMAC homo-polymer were evaluated in aqueous solutions via the DLS, SLS, ELS and ATR-FTIR methods. The self-assembly of inherently hydrophobic polyelectrolyte homo-polymers is of great interest thanks to their simple synthesis; however, controlling the morphologies of the resultant nanostructures has not been explored in depth. From a theoretical point of view, hydrophilic homo-PEs are expected to exist as single macromolecules in aqueous milieu [21]. DLS/SLS studies confirmed the literature data regarding the self-assembly behavior of homo-polymers/homo-PEs and revealed the existence of PVBTMAC single chains in aqueous media [21]. Particularly, the DLS/SLS data of Figure 1a highlights a symmetric and monomodal size distribution plot of the hydrophilic PVBTMAC homo-polymer, presumably corresponding to single homo-polymer chains (hydrodynamic radius (R_h) = 5 nm).

ELS data revealed the positive value of the PVBTMAC homo-PE (ζ_{pot} = +12 mV), which corresponds to the permanent positive charge of the quaternary amino group of the PVBTMAC homo-polymer. The scattered intensity, R_h, size, polydispersity index (PDI) and ζ_{pot} values of the PVBTMAC homo-polymer in aqueous media at 5×10^{-4} g·mL^{-1}, pH = 7 and 25 °C are gathered in Table 2 (first row).
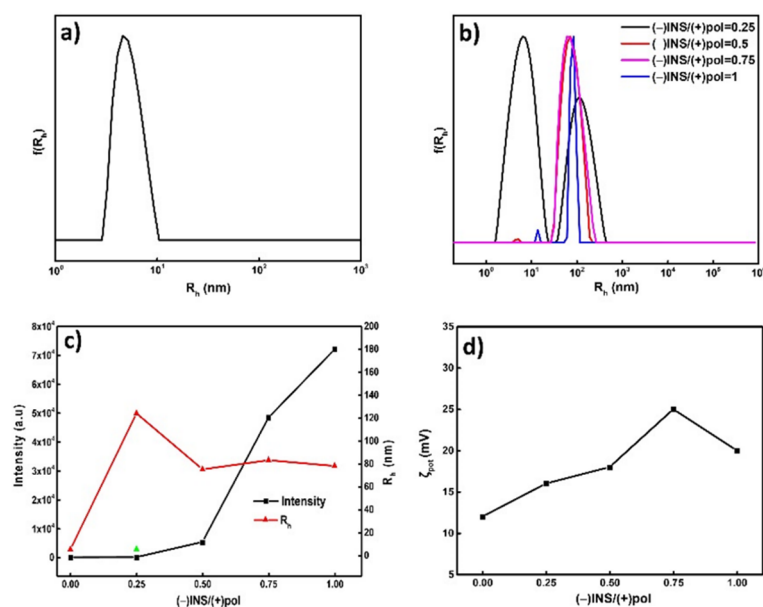
Figure 1. Size distributions from Contin analysis for (**a**) PVBTMAC homo-polymer and (**b**) PVBT-MAC/INS complexes at 0.01 M NaCl, (**c**) variations in scattering intensity and R_h (green triangle refers to single homo-polymer chains of 6 nm at $(-)$INS/$(+)$pol = 0.25) and (**d**) ζ_{pot} values as a function of $(-)$INS/$(+)$pol charge ratio for the PVBTMAC/INS complexes at pH = 7 and 25 °C.

Table 2. DLS, SLS and ELS results for the PVBTMAC homo-polymer and PVBTMAC/INS complexes at 0.01 M NaCl.

Sample	Intensity [a] (a.u)	R_h [a] (nm)	PDI [a]	ζ_{pot} [b] (mV)
PVBTMAC	21	5	0.56	+12
$(-)$INS/$(+)$pol = 0.25	33	6/124 *	0.51	+16
$(-)$INS/$(+)$pol = 0.50	5310	75	0.17	+18
$(-)$INS/$(+)$pol = 0.75	48,400	83	0.17	+25
$(-)$INS/$(+)$pol = 1	72,000	78	0.14	+20

[a] Determined by DLS/SLS at measuring angle 90°; [b] determined by ELS at measuring angle 90°; * multiple peaks observed in DLS size distribution.

A gamut of physicochemical techniques (DLS, SLS, ELS, ATR-FTIR and FS) was followed to verify the complexation efficiency of INS with the PVBTMAC homo-polymer and to detect any INS conformational changes after its complexation with the PVBTMAC solution. The comparison of size distributions and the variations in scattered intensity and R_h as a function of $(-)$INS/$(+)$pol charge ratio for the PVBTMAC/INS complexes are exhibited in Figure 1b,c, respectively. At $(-)$INS/$(+)$pol = 0.25 (Figure 1b, black line), where homo-polymer chains prevail in concentration over INS molecules, the PVBTMAC nanoassemblies coexist as pre-existing single PVBTMAC homo-polymer chains (R_h = 6 nm, Table 2) and PVBTMAC/INS complexes (R_h =124 nm, Table 2). Monomodal, symmetrical and narrow size distributions of the PVBTMAC/INS complexes are present from $(-)$INS/$(+)$pol = 0.5 (Figure 1b, red line) to $(-)$INS/$(+)$pol = 1 (Figure 1b, blue line), indicating the participation of all chains in the formation of the biohybrid complexes after complexation with INS molecules. As INS concentration increases from $(-)$INS/$(+)$pol ratio = 0.5 (R_h = 75 nm, Figure 1c) to $(-)$INS/$(+)$pol ratio = 1 (R_h = 78 nm, Figure 1c), the PVBTMAC/INS complexes become more compact, judging from their decreased size compared to $(-)$INS/$(+)$pol ratio = 0.25 (R_h = 124 nm, Figure 1c), denoting that their size depends on the concentration of INS in the solutions. Nevertheless, insignificant alterations in the R_h of the complexes are evident as INS concentration increases from $(-)$INS/$(+)$pol = 0.5 to $(-)$INS/$(+)$pol = 1. Notably, the PDI value of the PVBTMAC/INS complexes decreases

impressively from (−)INS/(+)pol = 0.25 to (−)INS/(+)pol = 1, highlighting the uniform size distribution of the resulting nanocarriers.

Additionally, DLS/SLS data manifested an astonishing increase in mass (according to the measured scattered light intensity from the examined solutions) of the PVBTMAC/INS complexes as INS increases (Table 2, Figure 1c), evidencing the successful complexation of INS with the PVBTMAC homo-polymer single chains. Notably, the scattered light intensity of the complexes increased more than 2000 times at (−)INS/(+)pol = 1 (in deficiency of the PVBTMAC homo-polymer) compared to the (−)INS/(+)pol = 0.25 charge ratio, uncovering the existence of complexes with a substantially greater mass. The remarkable increase in the mass of the complexes may be attributed to the formation of clusters of the homo-polymer/INS complexes at high protein concentrations.

DLS/SLS results indicate that the hydrophilic and hydrophobic domains of INS drastically regulated the co-assembly process, since the mass of the biohybrid complexes increased remarkably after the complexation with INS molecules. Overall, the obtained results are a consequence of a high complexation tendency between the components and a strongly synergistic co-assembly.

The strong positive ζ_{pot} values of the PVBTMAC/INS complexes detected by ELS measurements result from the permanently cationic PVBTMAC moieties decorating them, despite the existence of the negatively charged INS molecules. In particular, the obtained ζ_{pot} values display no significant differences in all charge ratios utilized (Table 2 and Figure 1d), implying the formation of cluster complexes, as mentioned earlier. The resulting nanocarriers possibly obtain an internal structure in which the cationic and hydrophilic PVBTMAC chains occupy the periphery of the complexes/clusters, while INS molecules are hidden in the internal part of the assemblies. A schematic representation of the electrostatic complexation of INS with the PVBTMAC homo-polymer chains is exhibited in Scheme 3.
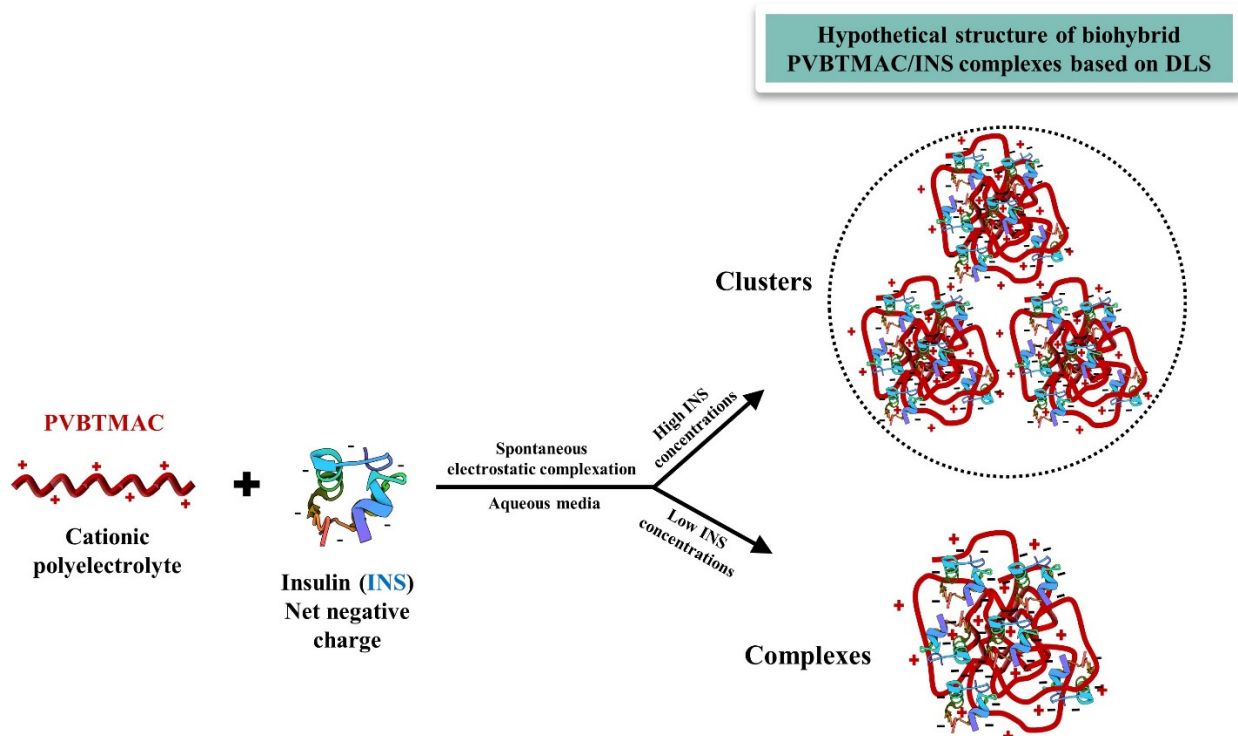
Scheme 3. Schematic illustration of the electrostatic complexation of INS with PVBTMAC homo-polymer.

The structural characterization of PVBTMAC and the ability of the particular homo-polymer to interact electrostatically with INS molecules to form complexes was elucidated using ATR-FTIR spectroscopy. The comparison of the ATR-FTIR spectra of the PVBT-MAC homo-polymer (black line), PVBTMAC/INS complexes at (−)INS/(+)pol = 1 (red

line) and solid INS (blue line) is provided in Figure 2. The ATR-FTIR spectrum of the PVBTMAC homo-polymer reveals several characteristic absorption bands corresponding to the expected molecular structure of the homo-polymer. The peaks at 3500–2720 cm^{-1} are attributed to stretching vibrations of aliphatic C–H region. The peaks centered at 1482 cm^{-1} correspond to the C=C stretching modes that are attributed to the aromatic ring of VBTMAC. Moreover, the peak at 1060 cm^{-1} refers to the C-N stretching bond vibrations in the amine groups of VBTMAC. Finally, the peaks at 890–620 cm^{-1} are attributed to the C-H out-of-plane bending vibrations of the phenyl ring of VBTMAC. The ATR-FTIR spectrum of solid INS presents characteristic absorption bands at 1650 cm^{-1}, 1522 cm^{-1} and 1449–1391 cm^{-1}, which are attributed to the amide I, II and III groups of the C=O stretching vibration [22]. Three characteristic absorption peaks at 1665 cm^{-1}, 1526 cm^{-1} and 1471–1354 cm^{-1} are depicted in the ATR-FTIR spectrum of the PVBTMAC/INS complexes at (−)INS/(+)pol = 1, which probably refer to the amide I, II and III groups of INS, verifying its existence in the mixed homo-polymer/INS solutions. Furthermore, a noticeable increase in the ATR-FTIR intensity of amide I and II peaks is shown in the case of PVBTMAC/INS complexes at (−)INS/(+)pol = 1, compared to solid INS, possibly denoting that some weak physical interactions were formed between INS and PVBTMAC during the preparation of the complexes and, thus, revealing some structural changes in the homo-polymer/protein system.
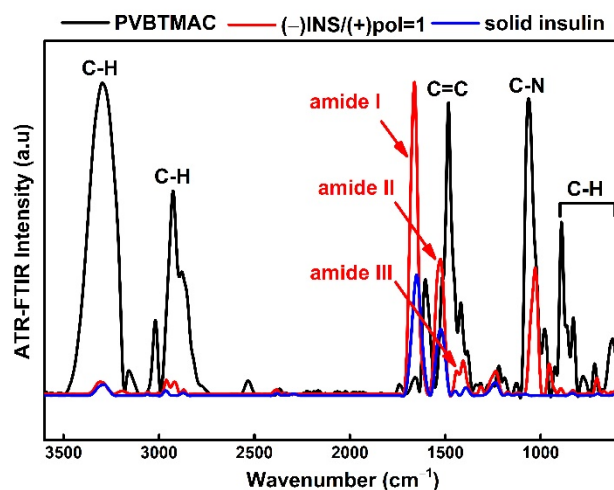
Figure 2. Comparative ATR-FTIR spectra of PVBTMAC homo-polymer, PVBTMAC/INS complexes at (−)INS/(+)pol = 1 and solid INS in the solid state.

FS measurements were conducted (excitation wavelength 280 nm) to further confirm the efficient complexation of INS with the homo-PE and to address any INS conformational changes after its complexation with the PVBTMAC homo-polymer [23]. The fluorescence spectrum of the PVBTMAC/INS complexes at different (−)INS/(+)pol charge ratios is presented in Figure 3a. Normalized fluorescence intensity versus (−)INS/(+)pol charge ratio at 307 nm (peak maximum) is also shown in Figure 3b. The shift in the wavelength of the maximum INS fluorescence is practically negligible (less than 5 nm), signifying weak conformational and structural alterations of INS after its complexation with PVBTMAC homo-PE. Specifically, the fluorescence intensity of the PVBTMAC/INS complexes increases linearly, as INS content rises in the complexes from (−)INS/(+)pol = 0.25 to (−)INS/(+)pol = 1, denoting that the increase in INS concentration did not lead to fluorescence quenching or precipitation of the formed PVBTMAC/INS nanocarriers.
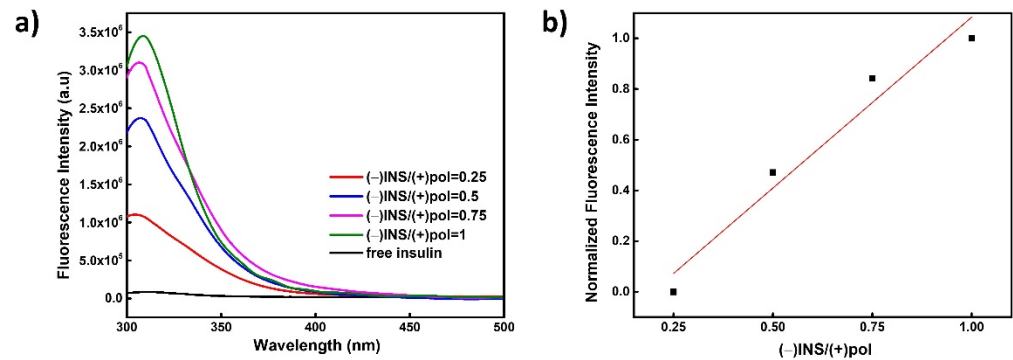
Figure 3. Comparative fluorescence spectra of (**a**) PVBTMAC/INS complexes and (**b**) normalized fluorescence intensity at 307 nm (peak maximum) as a function of $(-)$INS/$(+)$pol charge ratio.

3.3. Behavior of PVBTMAC/INS Complexes in the Presence of Salt

The addition of salt in aqueous PVBTMAC-based INS solutions under physiological conditions plays a central role in the solubility, size, structure and stability of the complexes [18,20,24]. In line with the literature data, a possible growth in the ionic strength of PE/protein solutions could result in (i) decomposition of the complexes, (ii) secondary aggregation, or even (iii) complex precipitation [25–27].

The dependence of R_h and scattered light intensity on the NaCl concentration for the PVBTMAC/INS complexes at $(-)$INS/$(+)$pol = 1 is depicted in Figure 4. The PVBTMAC/INS complexes present rather constant scattered light intensity values, as NaCl increases from 0.01 M to 0.1 M. As ionic strength rises from 0.1 M to 0.2 M, a sharp decline in the scattered intensity of the PVBTMAC/INS complexes is noticed. A less-steep and more-gradual decrease in intensity is evident, until the 0.5 M NaCl concentration. Overall, the dramatic drop in scattering intensity from 0.01 M to 0.5 M underlines the development of unstable complexes with reduced mass in the presence of NaCl.
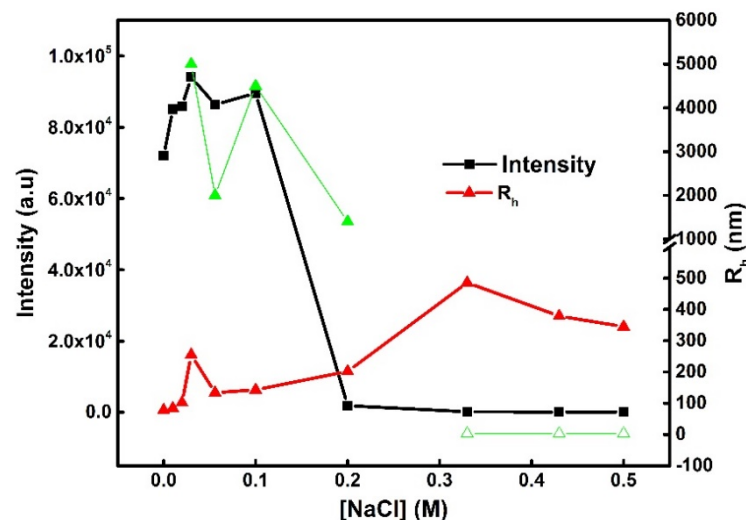
Figure 4. R_h and scattered light intensity as a function of ionic strength for PVBTMAC/INS complexes at $(-)$INS/$(+)$pol = 1. Solid green triangles refer to additional peaks of R_h = 1.5–5 μm observed in DLS distributions from 0.03 M to 0.2 M NaCl, while empty green triangles are attributed to extra DLS populations of R_h = 3 nm present from 0.33 M to 0.5 M NaCl.

With respect to size from the DLS measurements of the complexes, two populations are observed at low-salt concentrations in Figure 4. One with a larger size (1.5–5 μm, solid green triangles) and one with a smaller size (~200 nm, empty green triangles), but proportionally larger in scattering intensity. Respectively, two R_h populations are evident from 0.33 M to

0.5 M NaCl. The first presents a small size of ca. 3 nm (the empty green triangles) and the second with a higher size of 400 nm (the solid green triangles in the same salt-concentration range) and proportionally larger in scattering intensity. This observation demonstrates the presence of clusters of complexes and disintegration of the complexes, as salt concentration increases in the solution, since the larger populations of 1.5–5 μm are probably associated with the presence of swollen clusters, whereas the small-size population of 3 nm may be related to the existence of free INS molecules.

As far as the population with the higher-in-number scattering intensity is concerned, a substantial increase in the size of the PVBTMAC/INS nanocarriers is noticed, up to $R_h \sim 400$ nm, as ionic strength rises from 0.1 M to 0.33 M, followed by slight changes in R_h values until 0.5 M NaCl concentration. Specifically, the R_h of the complexes increases from 0.01 M to 0.5 M NaCl, followed by a parallel significant decrease in their mass. The low molecular weight salt leads to the liberation of the initially complexed charged groups of the PVBTMAC homo-polymer and INS as R_h increases, resulting in the enhancement of system's hydrophilicity and the swelling/disintegration behavior of the complexes.

### 3.4. FBS Interactions with PVBTMAC Homo-Polymer and PVBTMAC/INS Complexes

The stability of polymeric nanoparticulate biomaterials and polymer-based protein nanocarriers in serum components is essential to guarantee their use in protein delivery [19,20]. In the present contribution, the serum media selected for the physicochemical characterization of the PVBTMAC homo-polymer and PVBTMAC/INS complexes was FBS. Therefore, DLS stability studies in the presence of FBS for the PVBTMAC homo-polymer and PVBTMAC/INS complexes were conducted to investigate possible alterations in their physicochemical characteristics. The R_h and scattered intensity values of FBS and the PVBTMAC homo-polymer in PBS are provided in Table 3, along with the characteristics of FBS protein–PVBTMAC and FBS protein–PVBTMAC/INS mixtures. FBS stability studies of the PVBTMAC homo-polymer and PVBTMAC/INS complexes are displayed in Figure 5.

Table 3. Physicochemical characteristics of neat FBS, PVBTMAC homo-polymer in PBS, FBS-PVBTMAC and FBS-PVBTMAC/INS complexes mixtures, obtained from DLS measurements.

Sample	(−)INS/(+)pol	R_h (nm)	Intensity (a.u)
FBS	-	3/23/170 *	5760
PVBTMAC	-	5	30
PVBTMAC+FBS:PBS (1/9 *v/v*)	-	5/14/113 *	1948
PVBTMAC/INS+FBS:PBS (1/9 *v/v*)	0.25	3/10/79 *	772
PVBTMAC/INS+FBS:PBS (1/9 *v/v*)	0.5	3/11/96 *	849
PVBTMAC/INS+FBS:PBS (1/9 *v/v*)	0.75	3/10/96 *	897
PVBTMAC/INS+FBS:PBS (1/9 *v/v*)	1	3/9/80 *	1116

* Multiple peaks observed in DLS size distribution. The "-" represents absence of information.

The comparison of intensity-weighted size distributions of the PVBTMAC homo-polymer in PBS (red line) and FBS (black line) is exhibited in Figure 5a. Figure 5b exhibits the intensity-weighted size distribution of the PVBTMAC+FBS:PBS (1/9 *v/v*) mixtures. Furthermore, the size distributions of the PVBTMAC/INS+FBS:PBS (1/9 *v/v*) mixtures at different (−)INS/(+)pol charge ratios are depicted in Figure 5c–f. Trimodal size distributions of FBS proteins appear with peaks at ca. 3 nm, 23 nm and 170 nm (Table 3), highlighting the formation of single proteins (i.e., low values of R_h) and larger size aggregates, respectively. The size-distribution plot of the PVBTMAC homo-polymer in PBS media underlines the existence of single chains (Figure 5a, red line). After 1 h of PVBTMAC incubation with FBS, DLS stability studies evidenced a coexistence of PVBTMAC single chains or free FBS proteins and FBS aggregates (Figure 5b, Table 3), compared to PVBTMAC homo-polymer in PBS (Table 3), denoting weak interactions between the homo-polymer and FBS.
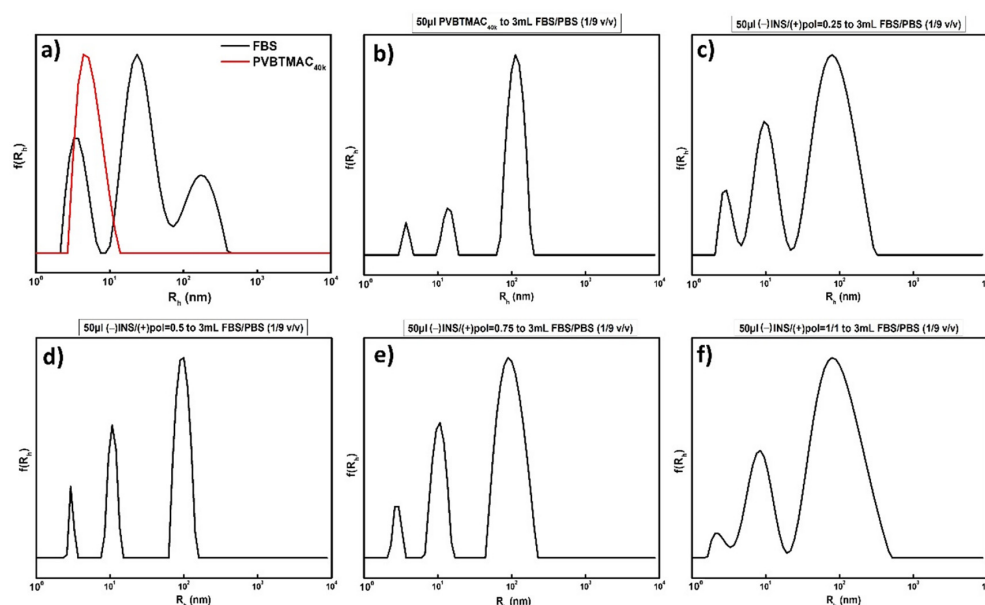
Figure 5. (**a**) Comparative size distributions of FBS (black line) and PVBTMAC homo-polymer in PBS (red line) and intensity-weighted size distributions of (**b**) PVBTMAC+FBS:PBS (1/9 *v/v*), (**c**) PVBTMAC/INS+FBS:PBS (1/9 *v/v*) at (−)INS/(+)pol = 0.25, (**d**) PVBTMAC/INS+FBS:PBS (1/9 *v/v*) at (−)INS/(+)pol = 0.5, (**e**) PVBTMAC/INS+FBS:PBS (1/9 *v/v*) at (−)INS/(+)pol = 0.75, and (**f**) PVBTMAC/INS+FBS:PBS (1/9 *v/v*) at (−)INS/(+)pol = 1.

Free proteins and slightly increased-size PVBTMAC/INS complexes (compared to the complexes before mixing with serum) were exhibited, after mixing the PVBTMAC/INS complexes with serum components, at almost all (−)INS/(+)pol charge ratios (except at (−)INS/(+)pol = 0.25, Table 3), implying negligible interactions between PVBTMAC/INS complexes and FBS.

Regarding measured scattered-light-intensity values, a dramatic decline in FBS is evident compared to all FBS protein-PVBTMAC and FBS protein-PVBTMAC/INS mixtures (Table 3), suggesting a noteworthy reduction in the mass of FBS aggregates, due to the presence of the PVBTMAC homo-polymer. The parallel decrease in scattered light intensity of the PVBTMAC/INS complexes, after mixing with FBS at all charge ratios (compared to the complexes before mixing with serum), apparently leads to partial dissociation of the initially formed PVBTMAC/INS complexes. Notably, the small R_h value (ca. 100 nm in all cases) of the supramolecular aggregates of INS nanocarriers and serum proteins is one of the most important factors in their utility for a wide variety of biological applications [28]. Collectively, all data manifested weak interactions between FBS and PVBTMAC homo-polymer and PVBTMAC/INS complexes.

4. Conclusions

Novel biohybrid nanosystems were successfully developed utilizing the RAFT-synthesized biocompatible, cationic PVBTMAC homo-polyelectrolyte for the electrostatic complexation with INS.

The hydrophilic PVBTMAC polyelectrolyte formed single chains at 0.01 M NaCl. The determined physicochemical characteristics of the PVBTMAC/INS complexes depended on (−)INS/(+)pol charge ratio and verified the efficient complexation of INS with the PVBTMAC homo-polymer chains. Specifically, the presence of hydrophobic and hydrophilic moieties of INS into the homo-polymer chains altered the structural characteristics of PVBTMAC/INS complexes, by modulating the organization of the PE components.

Likewise, neat PVBTMAC homo-polymer and PVBTMAC/INS nanocarriers demonstrated good serum stability in the presence of FBS proteins. Moreover, FS studies revealed

no INS conformational changes after its complexation with the cationic PVBTMAC polyelectrolyte.

The physicochemical evaluation of the bio-hybrid PVBTMAC/INS complexes conducted in this study, sheds light on the (i) assembling behavior and (ii) electrostatic interaction between an oppositely charged homo-PE and biomacromolecules. The formed nano-sized PVBTMAC INS electrostatic complexes set the stage for further biopharmaceutical evaluation to promote their potential use as insulin delivery systems.

References

1. Armstrong, J.P.; Olof, S.N.; Jakimowicz, M.D.; Hollander, A.P.; Mann, S.; Davis, S.A.; Miles, M.J.; Patil, A.J.; Perriman, A.W. Cell paintballing using optically targeted coacervate microdroplets. *Chem. Sci.* **2015**, *6*, 6106–6111. [CrossRef] [PubMed]
2. Eghbal, N.; Choudhary, R. Complex coacervation: Encapsulation and controlled release of active agents in food systems. *Lwt* **2018**, *90*, 254–264.
3. Huang, G.Q.; Du, Y.L.; Xiao, J.X.; Wang, G.Y. Effect of coacervation conditions on the viscoelastic properties of N,O-carboxymethyl chitosan–gum Arabic coacervates. *Food Chem.* **2017**, *228*, 236–242. [CrossRef] [PubMed]
4. Li, Z.; Wang, Y.; Pei, Y.; Xiong, W.; Zhang, C.; Xu, W.; Liu, S.; Li, B. Curcumin encapsulated in the complex of lysozyme/carboxymethylcellulose and implications for the antioxidant activity of curcumin. *Food Res. Int.* **2015**, *75*, 98–105. [CrossRef]
5. Cooper, C.; Dubin, P.; Kayitmazer, A.; Turksen, S. Polyelectrolyte–protein complexes. *Curr. Opin. Colloid Interface Sci.* **2005**, *10*, 52–78.
6. Kayitmazer, A.B.; Seeman, D.; Minsky, B.B.; Dubin, P.L.; Xu, Y. Protein–polyelectrolyte interactions. *Soft Matter* **2013**, *9*, 2553–2583. [CrossRef]
7. Hess, M.; Jones, R.G.; Kahovec, J.; Kitayama, T.; Kratochvíl, P.; Kubisa, P.; Mormann, W.; Stepto, R.; Tabak, D.; Vohlídal, J. Terminology of polymers containing ionizable or ionic groups and of polymers containing ions (IUPAC Recommendations 2006). *Pure Appl. Chem.* **2006**, *78*, 2067–2074. [CrossRef]
8. Winkler, R.G.; Cherstvy, A.G. Strong and weak polyelectrolyte adsorption onto oppositely charged curved surfaces. In *Polyelectrolyte Complexes in the Dispersed and Solid State I: Principles and Theory*; Müller, M., Ed.; Springer: Berlin/Heidelberg, Germany, 2014; Volume 255, pp. 1–56.
9. Horn, J.M.; Kapelner, R.A.; Obermeyer, A.C. Macro-and microphase separated protein-polyelectrolyte complexes: Design parameters and current progress. *Polymers* **2019**, *11*, 578. [CrossRef]
10. Semenyuk, P.; Muronetz, V. Protein interaction with charged macromolecules: From model polymers to unfolded proteins and post-translational modifications. *Int. J. Mol. Sci.* **2019**, *20*, 1252. [CrossRef]
11. Wang, H.; Qian, C.; Roman, M. Effects of pH and salt concentration on the formation and properties of chitosan–cellulose nanocrystal polyelectrolyte–macroion complexes. *Biomacromolecules* **2011**, *12*, 3708–3714. [CrossRef]
12. Bayat, A.; Dorkoosh, F.A.; Dehpour, A.R.; Moezi, L.; Larijani, B.; Junginger, H.E.; Rafiee-Tehrani, M. Nanoparticles of quaternized chitosan derivatives as a carrier for colon delivery of insulin: Ex vivo and in vivo studies. *Int. J. Pharm.* **2008**, *356*, 259–266. [CrossRef]
13. Sadeghi, A.M.M.; Dorkoosh, F.A.; Avadi, M.R.; Weinhold, M.; Bayat, A.; Delie, F.; Gurny, R.; Larijani, B.; Rafiee-Tehrani, M.; Junginger, H.E. Permeation enhancer effect of chitosan and chitosan derivatives: Comparison of formulations as soluble polymers and nanoparticulate systems on insulin absorption in Caco-2 cells. *Eur. J. Pharm. Biopharm.* **2008**, *70*, 270–278. [CrossRef]
14. Lu, X.; Gao, H.; Li, C.; Yang, Y.W.; Wang, Y.; Fan, Y.; Wu, G.; Ma, J. Polyelectrolyte complex nanoparticles of amino poly (glycerol methacrylate)s and insulin. *Int. J. Pharm.* **2012**, *423*, 195–201. [CrossRef]
15. Thompson, C.; Tetley, L.; Uchegbu, I.; Cheng, W. The complexation between novel comb shaped amphiphilic polyallylamine and insulin—towards oral insulin delivery. *Int. J. Pharm.* **2009**, *376*, 46–55.

16. Jintapattanakit, A.; Junyaprasert, V.B.; Mao, S.; Sitterberg, J.; Bakowsky, U.; Kissel, T. Peroral delivery of insulin using chitosan derivatives: A comparative study of polyelectrolyte nanocomplexes and nanoparticles. *Int. J. Pharm.* **2007**, *342*, 240–249. [CrossRef]

17. Lou, B.; Beztsinna, N.; Mountrichas, G.; van den Dikkenberg, J.B.; Pispas, S.; Hennink, W.E. Small nanosized poly (vinyl benzyl trimethylammonium chloride) based polyplexes for siRNA delivery. *Int. J. Pharm.* **2017**, *525*, 388–396. [CrossRef]

18. Haladjova, E.; Mountrichas, G.; Pispas, S.; Rangelov, S. Poly (vinyl benzyl trimethylammonium chloride) Homo and Block Copolymers Complexation with DNA. *J. Phys. Chem. B* **2016**, *120*, 2586–2595. [CrossRef]

19. Pippa, N.; Kaditi, E.; Pispas, S.; Demetzos, C. PEO-b-PCL–DPPC chimeric nanocarriers: Self-assembly aspects in aqueous and biological media and drug incorporation. *Soft Matter* **2013**, *9*, 4073–4082. [CrossRef]

20. Chroni, A.; Forys, A.; Sentoukas, T.; Trzebicka, B.; Pispas, S. Poly [(vinyl benzyl trimethylammonium chloride)]-based nanoparticulate copolymer structures encapsulating insulin. *Eur. Polym. J.* **2022**, *169*, 111158. [CrossRef]

21. Du, J.; Willcock, H.; Patterson, J.P.; Portman, I.; O'Reilly, R.K. Self-Assembly of Hydrophilic Homopolymers: A Matter of RAFT End Groups. *Small* **2011**, *7*, 2070–2080. [CrossRef]

22. Delbeck, S.; Heise, H.M. Quality assurance of commercial insulin formulations: Novel assay using infrared spectroscopy. *J. Diabetes Sci. Technol.* **2021**, *15*, 865–873. [CrossRef]

23. Correia, M.; Neves-Petersen, M.T.; Jeppesen, P.B.; Gregersen, S.; Petersen, S.B. UV-light exposure of insulin: Pharmaceutical implications upon covalent insulin dityrosine dimerization and disulphide bond photolysis. *PLoS ONE* **2012**, *7*, e50733. [CrossRef]

24. Chroni, A.; Forys, A.; Trzebicka, B.; Alemayehu, A.; Tyrpekl, V.; Pispas, S. Poly [oligo (ethylene glycol) methacrylate]-b-poly [(vinyl benzyl trimethylammonium chloride)] Based Multifunctional Hybrid Nanostructures Encapsulating Magnetic Nanoparticles and DNA. *Polymers* **2020**, *12*, 1283. [CrossRef]

25. Karayianni, M.; Pispas, S.; Chryssikos, G.D.; Gionis, V.; Giatrellis, S.; Nounesis, G. Complexation of lysozyme with poly (sodium (sulfamate-carboxylate) isoprene). *Biomacromolecules* **2011**, *12*, 1697–1706. [CrossRef]

26. Quinn, R.; Andrade, J.D. Minimizing the aggregation of neutral insulin solutions. *J. Pharm. Sci.* **1983**, *72*, 1472–1473. [CrossRef]

27. Lee, A.S.; Bütün, V.; Vamvakaki, M.; Armes, S.P.; Pople, J.A.; Gast, A.P. Structure of pH-dependent block copolymer micelles: Charge and ionic strength dependence. *Macromolecules* **2002**, *35*, 8540–8551. [CrossRef]

28. Biswas, A.K.; Islam, M.R.; Choudhury, Z.S.; Mostafa, A.; Kadir, M.F. Nanotechnology based approaches in cancer therapeutics. *Adv. Nat. Sci. Nanosci. Nanotechnol.* **2014**, *5*, 043001.